Breast implant surface texture impacts host tissue response

Michael Atlan, Gina Nuti, Hongpeng Wang, Sherri Decker, Tracyann Perry

Journal of the Mechanical Behavior of Biomedical Materials 88 (2018) 377–385

Contents lists available at ScienceDirect

Journal of the Mechanical Behavior of Biomedical Materials

journal homepage: www.elsevier.com/locate/jmbbm

Breast implant surface texture impacts host tissue response

Michael Atlan[a], Gina Nuti[b], Hongpeng Wang[b], Sherri Decker[b], TracyAnn Perry[b,*]

[a] APHP Hopital Tenon, Université Pierre et Marie Curie Paris VI, Maitre de conférence des Universités Praticien Hospitalier, 4 rue de la Chine, 75020 Paris, France
[b] Allergan plc, 2525 Dupont Dr, Irvine, CA, USA

ARTICLE INFO

Keywords:
Breast implants
X-ray computed tomography
Scanning electron microscopy
Surface texture
Tissue adherence

ABSTRACT

Background: Surface texture of a breast implant influences tissue response and ultimately device performance. Characterizing differences among available surface textures is important for predicting and optimizing performance.
Methods: Scanning electron microscopy (SEM) and X-ray computed tomography (CT)-imaging were used to characterize the topography and surface area of 12 unique breast implant surface textures from seven different manufacturers. Samples of these surface textures were implanted in rats, and tissue response was analyzed histologically. In separate experiments, the force required to separate host tissue from the implant surface texture was used as a measure of tissue adherence.
Results: SEM imaging of the top and cross section of the implant shells showed that the textures differed qualitatively in evenness of the surface, presence of pores, size and openness of the pores, and the depth of texturing. X-ray CT imaging reflected these differences, with the texture surface area of the anterior of the shells ranging from 85 to 551 mm^2, which was 8–602% greater than that of a flat surface. General similarities based on the physical structure of the surfaces were noted among groups of textures. In the rat models, with increasing surface texture complexity, there was increased capsule disorganization, tissue ingrowth, and tissue adherence.
Conclusions: Surface area and topography of breast implant textures are important factors contributing to tissue ingrowth and adherence. Based on surface area characteristics and measurements, it is possible to group the textures into four classifications: smooth/nanotexture (80–100 mm^2), microtexture (100–200 mm^2), macrotexture (200–300 mm^2), and macrotexture-plus ($>$ 300 mm^2).

1. Introduction

Breast implants are widely used for cosmetic augmentation and post-mastectomy breast reconstruction. Many types of breast implants are available that differ across a range of physical characteristics, such as shape, size, gel material, and surface texture (Atlan et al., 2016; Maxwell et al., 2014) and also differ in the chemical composition of implant components, such as the elastomer shell (Kappel et al., 2014). Selecting the appropriate implant among the many options depends on personal preferences of the physician and patient, and the desired aesthetic outcome. However, the physical characteristics of an implant may influence clinical performance and should be considered during the selection process. This is particularly true for implant surface texture, which plays a key role in shaping breast tissue response (Harvey et al., 2013).

Following implantation, the host tissue recognizes the breast implant device as a foreign body and initiates an immune response that can result in formation of a collagen fiber capsule around the implant (Efanov et al., 2017; Sheikh et al., 2015). Capsule formation is a normal tissue response but can become problematic when the capsule contracts around the implant, making the breast hard and deformed, a complication known as capsular contracture (Hakelius and Ohlsen, 1992). It is thought that collagen fiber alignment plays a key role in capsular contracture, and that disruption of such fiber alignment may lead to reductions in the incidence and severity of capsular contracture (Bui et al., 2015). The surface texture of the breast implant can impact capsule formation, specifically the organization of the capsule's collagen fibers and adherence of the tissue to the device (Barr et al., 2009; Harvey et al., 2013; Valencia-Lazcano et al., 2013). A smooth silicone implant leads to formation of a nonadherent dense capsule with highly aligned and organized collagen fibers (Brohim et al., 1992; Danino et al., 2018). However, when a device with a textured surface is implanted, tissue ingrowth into the texture surface can disrupt the alignment of the surrounding capsule, which has been associated with lower

* Corresponding author.
E-mail addresses: drmichaelatlan@gmail.com (M. Atlan), Nuti_Gina@Allergan.com (G. Nuti), Wang_Hongpeng@Allergan.com (H. Wang), Sherri.Decker-Gragson@Allergan.com (S. Decker), tracyann.perry07@gmail.com, racyann.perry07@gmail.com (T. Perry).

https://doi.org/10.1016/j.jmbbm.2018.08.035
Received 11 May 2018; Received in revised form 15 August 2018; Accepted 26 August 2018
Available online 28 August 2018

rates of clinically significant capsular contracture and malposition compared with smooth surface implants (Barnsley et al., 2006; Brohim et al., 1992; Clugston et al., 1994; Derby and Codner, 2015; Hakelius and Ohlsen, 1992, 1997; Headon et al., 2015). Deeper and more complex textures promote increased tissue ingrowth (Brohim et al., 1992; Danino et al., 2001; Minami et al., 2006). As a result, the force required to break the interface between the capsule and implant is greater than less complex textures, which may reduce the risk of device rotation (del Rosario et al., 1995; Maxwell et al., 2014). Greater tissue ingrowth has also been correlated with reduced synovial-like metaplasia in human breast capsules due to the reduction in movement between the implant and surrounding stroma (Yeoh et al., 1996).

Breast implant manufacturers continue to develop new implant surface textures using varying methodologies in an effort to stabilize the implant in the pocket through increased coefficient of friction or enhanced integration of the device with breast tissue (Derby and Codner, 2015; Harvey et al., 2013). Herein, we describe the use of scanning electron microscopy (SEM) and X-ray computed tomography (CT) imaging to characterize the topography and surface area of 12 unique breast implant surface textures from 7 different manufacturers and evaluate how surface texture influences capsule formation and tissue adherence in rats.

2. Materials and methods

2.1. Breast implants

The surface texture of shells from 12 different breast implant devices were evaluated (Table 1). Each of these implants are silicone coated except for Polytech Microthane, which is polyurethane coated to create an irregular sponge-like surface. The processes for creating surface texture on the silicone implants differ across manufacturers. For example, the Microcell, Biocell, Nagotex, and Cristalline textures are created using different lost-salt techniques, in which a layer of fine granular salt is applied to the silicone shell before curing, and then removed by rinsing with water after curing. The lost-salt technique used to prepare Allergan Biocell was designed to produce overhangs at the opening of the pores to promote greater tissue adherence. In comparison, the Mentor Siltex texture is generated by a pressure imprint-stamping technique, and the Sientra True texture is produced by an undisclosed technique that does not involve use of salt or pressure stamping (Barr et al., 2017; Chao et al., 2016; Maxwell and Gabriel, 2017).

2.2. Breast implant surface imaging

SEM was used to image the surface of the breast implant textures using a single shell per implant type (Atlan et al., 2016; Barr et al., 2017). One 10-mm diameter disk was cut from the anterior of the shell of each breast implant device and used to capture a top and cross-sectional view of the surface texture. Samples were secured to a specimen mount with carbon adhesive, sputter coated with gold at 25 mA for 2 min, and imaged with a Hitachi S-3400N Tungsten Filament Scanning Electron Microscope using an electron beam accelerating voltage of 5 kV and aperture of 0. Images were captured at 40× and 100× magnification for the top view and 40× magnification for the cross section.

Table 1
Manufacturer and surface texture of breast implant devices.

Manufacturer	Implant type
Allergan plc (Dublin, Ireland)	Smooth texture
	Microcell texture
	Biocell texture
Eurosilicone S.A.S. (Apt, France)	Cristalline texture
Mentor (Irvine, CA, USA)	Siltex texture
Motiva/Establishment Labs (Alajuela, Costa Rica)	SilkSurface texture
	VelvetSurface texture
Nagor (Glasgow, Scotland)	Nagotex texture
Polytech Health & Aesthetics (Dieburg, Germany)	MESMOsensitive texture
	POLYtxt texture
	Microthane texture
Sientra (Santa Barbara, CA, USA)	True texture

In a separate experiment designed to explore additional methods of pore characterization, SEM images were taken of 2 similar pore textures of different surface areas (i.e., Allergan Microcell and Allergan Biocell) to quantify pore density, pore opening area, surface openness, and texture depth. Details of the methods used in this experiment can be found in the Supplementary material.

X-ray CT was used to determine the surface area of the breast implant textures. Eight 10-mm diameter disks were cut from the shell of each breast implant device, four from the anterior and four from the posterior of the shell. The entire geometry of each disk was acquired by taking a series of 2-dimensional X-ray images (slices) while the implant disk was concentrically rotated 360° in the X-ray beam. These slices containing information about the implant disk's position (with 15 µm voxel resolution) and density (gray scale) were used as the basis for digital 3-dimensional reconstruction of the sample's volume data (Fig. 1a) (ASTM International, 2011; Landis and Keane, 2010). All internal and external surfaces of the implant sample were extracted from this CT volume data. The spatial precision of the CT projection data was checked by a certified CT test standard (ruby bar with a length of 4.0432 ± 0.0020 mm; GE Sensing & Inspection Technologies, GmbH, Wunstorf, Germany).

A vertical cross section of the X-ray CT image was used to measure the thickness of the non-textured area, which was defined as the location starting from the bottom of the disk to the flat area near the top of the disk or the lowest point of any protrusions present on the surface (Fig. 1b). The thickness of the non-textured area was measured in three areas of the cross section and averaged. The average thickness of the non-textured area was used to calculate the surface area of the non-textured area (sides and bottom of disk) according to the formula for the area of a cylinder based on the assumption that the bottom of the disk was a flat surface. The resulting surface area of the non-textured surface was subtracted from the total surface area of the disk (obtained using CT software) to produce a surface area measurement for the textured surface (top of disk) (Fig. 1c). The surface area of the textured surface was calculated in terms of mm^2 as well as the percentage higher than that of a flat surface. The textured surface of the disk can be seen as the top circle of a cylinder; therefore, the surface area of a flat surface texture would be the surface area of a circle with a 5 mm radius (i.e., 79 mm^2).

2.3. Capsule formation

The protocols used in the animal studies were approved by the Institutional Animal Care and Use Committee. This study is conducted in compliance with the National Institutes of Health Guide for the Care and Use of Laboratory Animals, and Allergan, plc standard operating procedures. Capsule formation following subcutaneous implantation of disks cut from the shells of the different breast implants was evaluated in male Sprague -Dawley rats (Charles River Laboratories; Wilmington, MA). A total of six 30-mm disks (3 each from the anterior and posterior of the implant shell) were evaluated for each implant surface texture. The implantation scheme comprises three disks per rat in one of four locations along the torso (right cranial, right caudal, left cranial, and left caudal). The disks were implanted under anesthesia with 4% isoflurane in 2 L/min oxygen, with the textured surface of the disk facing the muscle. Six weeks later, the disk and surrounding tissue were explanted, and the tissue in contact with the textured surface of the disk was excised. Tissue samples were fixed in 10% neutral-buffered formalin, then processed and embedded in paraffin. Sections were cut at

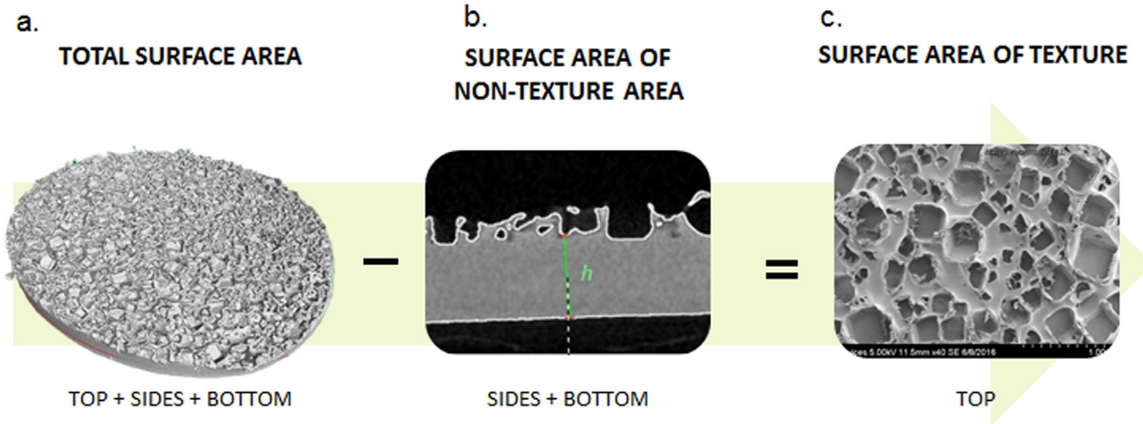

Fig. 1. Method for calculating surface area of the textured surface of a 10-mm diameter disk taken from the shell of a breast implant. (a) The implant shell disk was imaged using X-ray CT, and with the CT software, a threshold applied to distinguish between material and air was used to produce a value for total surface area of the disk. (b) The thickness of the non-textured portion of the shell was measured and used to calculate the surface area of the non-textured area ($A = 2\pi rh + 2\pi r^2$, where A is surface area, r is radius, and h is height.). (c) The surface area of texture was calculated by subtracting the surface area of the non-textured area from the total surface area based on the assumption that the bottom of the disk was a flat surface.

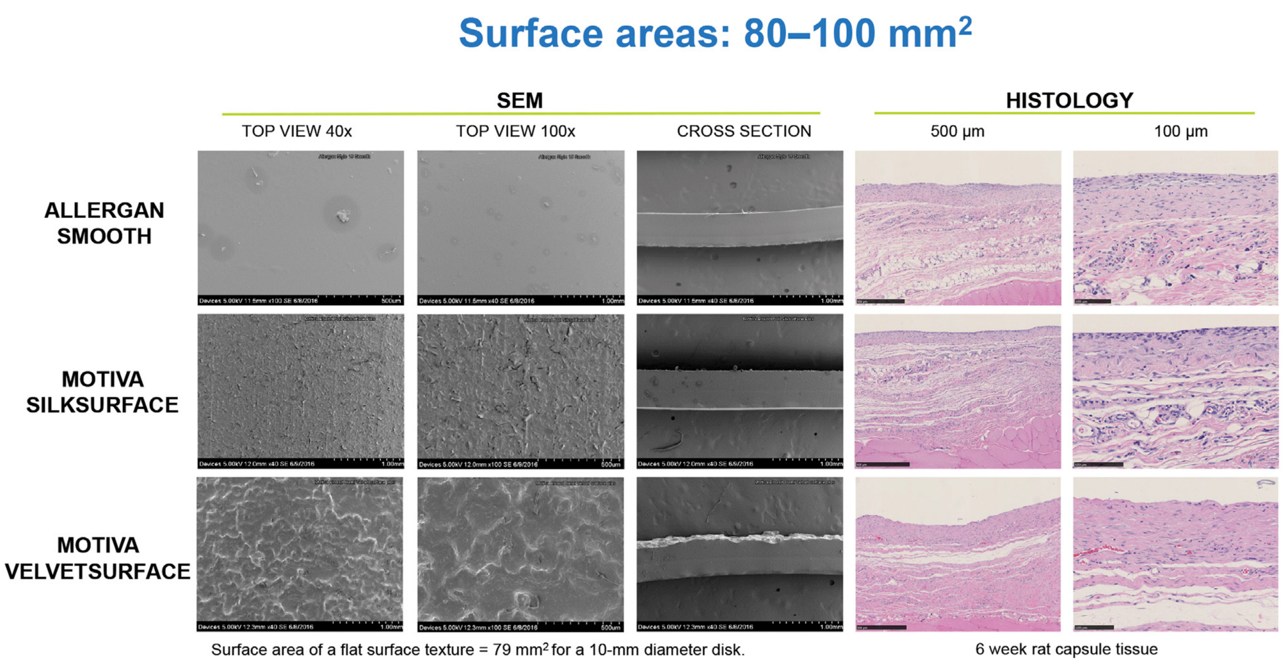

Fig. 2. Left panels show SEM images of the top view (40× and 100×) and cross section of Allergan Smooth, Motiva SilkSurface, and Motiva VelvetSurface textures. Surface areas range from 80 to 100 mm^2. Right panels show representative H&E-stained slides of the capsule at the tissue-implant interface at 6 weeks after subcutaneous implantation of 30-mm disks of each surface texture into Sprague-Dawley rats. The scale bars at the bottom of the histology figures represent 500 µm and 100 µm, respectively.

5 µm and stained with hematoxylin and eosin (H&E) to qualitatively visualize the gross morphology of the tissue-implant surface interface, including the arrangement of collagen fibers of the capsule. Stained slides were imaged using bright-field microscopy.

2.4. Tissue adherence

The strength of the interaction between the breast implant shell and fibrous capsule was evaluated by peel test in male Sprague-Dawley rats. Strips of the anterior of the implant shells measuring 1 cm in width and 4 cm in length were implanted under anesthesia with 4% isoflurane in 2 L/min oxygen. Each rat received two subcutaneous implants along the dorsal surface, one on the right side and the other on the left side, with the texture surface of the implant facing toward the muscle (n = 8 per implant surface texture). Six weeks later the strip and surrounding tissue capsule were explanted.

The strength of tissue adherence to the implant surface texture was measured by the peak force that was required to separate the surrounding tissue from the shell material. Testing was performed using an ADMET 5601 Universal Testing Machine (ADMET; Norwood, MA) with a 22 lb load cell. The excised tissue capsule and attached implant strip were each fastened into separate grips on the mechanical tester and pulled apart at a rate of 2 mm/s. Testing continued until the tissue was completely separated from the implant strip. Peak force, or maximum value on the force-displacement curve was recorded.

2.5. Statistical analyses

The surface area of the implant textures determined by X-ray CT was evaluated using descriptive statistics. Comparisons between the

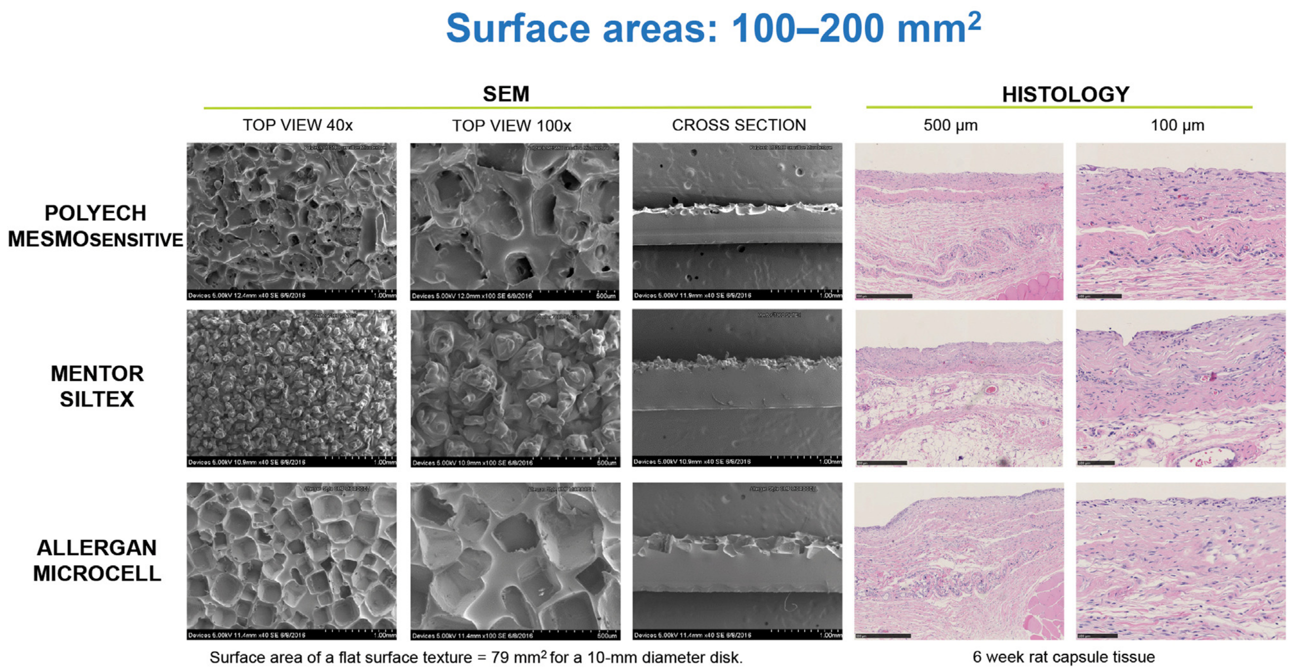

Fig. 3. Left panels show SEM images of the top view (40 × and 100 ×) and cross section of Polytech MESMOsensitive, Mentor Siltex, and Allergan Microcell textures. Surface areas range from 100 to 200 mm^2. Right panels show representative H&E-stained slides of the capsule at the tissue-implant interface at 6 weeks after subcutaneous implantation of 30-mm disks of each surface texture into Sprague-Dawley rats. The scale bars at the bottom of the histology figures represent 500 µm and 100 µm, respectively.

texture surface area of the anterior versus posterior of the implant shell were performed using a 2-sample *t*-test, with significance achieved at a $P \le 0.05$. Differences in tissue adherence force were evaluated using an analysis of variance model with Tukey's correction.

3. Results

3.1. Breast implant surface imaging

SEM imaging revealed the implant textures differed visually in evenness of the surface, presence of pores, size and openness of the pores, and the depth of texturing. Nonetheless, general similarities were noted among groups of textures. Allergan Smooth, Motiva SilkSurface, and Motiva VelvetSurface textures appeared relatively flat, with little or no depth in the texturing, but differed in the unevenness of the surface (Fig. 2; SEM panels). Polytech MESMOsensitive, Mentor Siltex, and Allergan Microcell all exhibited pores or nodules and showed increased complexity compared with Allergan Smooth, Motiva SilkSurface, and Motiva VelvetSurface textures (Fig. 3; SEM panels). The remaining textures, in turn, showed increasing surface unevenness and depth of texture that could be grouped according to similarities in appearance (Figs. 4 and 5; SEM panels).

To quantify differences across the implant textures, X-ray CT was used to measure the surface area of the texture. The texture surface area of a 10-mm diameter disk from the anterior of the shell from the 12 breast implant devices ranged from 85 to 551 mm^2, and correspondingly, their surface texture was 8–602% greater than that of a flat surface (79 mm^2) (Table 2). The texture surface area did not differ significantly between the anterior and posterior for most implant devices, except for Mentor Siltex (125 vs 143 mm^2; $P = 0.02$), Allergan Biocell (213 vs 248 mm^2; $P < 0.01$), and Polytech POLYtxt (347 vs 431 mm^2; $P = 0.01$) which had more texture surface area on the posterior of the shell, and Nagor Nagotex (337 vs 278 mm^2; $P < 0.01$), which had more texture surface area on the anterior of the shell.

Results of the experiment designed to compare the shell surface features of implants based on calculations of pore density, pore opening area, surface openness, and texture depth showed that these features can be used to distinguish implant surface textures. Details of the results of this experiment can be found in the Supplementary material.

3.2. Capsule formation

Capsule formation in response to the implant surface texture was qualitatively evaluated 6 weeks after subcutaneous implantation of 30-mm disks cut from the shell of each implant device. Representative H&E-stained sections illustrating the gross morphology of the tissue-implant interface are shown in Figs. 2–5 (histology panels).

Overall, the morphology of the capsule tissue aligned with the topography of the implant surface regardless of whether the disks were from the anterior or posterior of the implant shell. Capsule morphology was similar across groups of surface textures with the larger surface area textures showing disorganized alignment of collagen fibers. The tissue along the implant-tissue interface for the textures with the smallest surface area (Allergan Smooth, Motiva SilkSurface, and Motiva VelvetSurface) was mostly flat, with the collagen fibers of the capsule aligned parallel to the surface. Polytech MESMO, Mentor Siltex, and Allergan Microcell had small tissue projections scattered along the interface adding a small degree of disorganization to the collagen fiber alignment. Allergan Biocell, Sientra True, Eurosilicone Cristalline, Nagor Nagotex, Polytech Polytxt, and Polytech Microthane showed larger, more prominent tissue projections, resulting in irregular arrangement of collagen fibers and creating a more disorganized capsule morphology. The capsule morphology of Polytech Microthane contained fragments of texture material (see clear material in Fig. 5) embedded throughout the capsule tissue; this was not observed with any other implants.

3.3. Tissue adherence

The peak force required for separation of the surrounding tissue capsule from the different surface textures was assessed using a peel test at 6 weeks following implantation. As shown in Fig. 6, the peak force

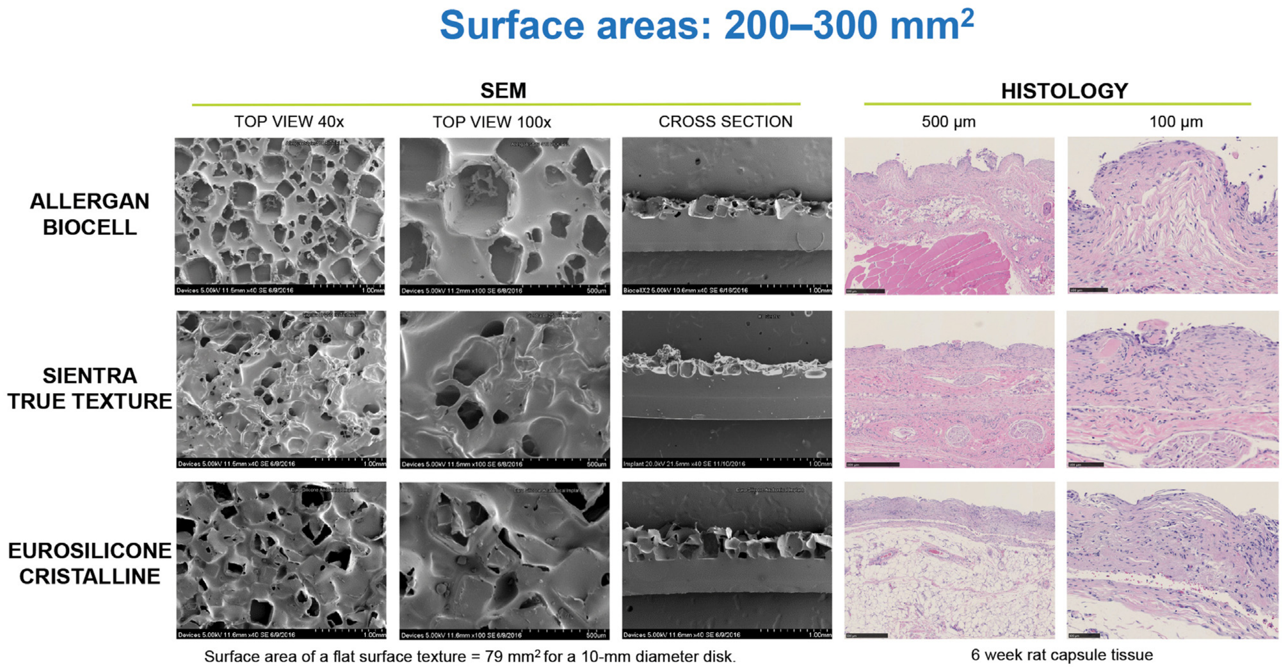

Fig. 4. Left panels show SEM images of the top view (40× and 100×) and cross section of Allergan Biocell, Sientra True, and Eurosilicone Cristalline textures. Surface areas range from 200 to 300 mm^2. Right panels show representative H&E-stained slides of the capsule at the tissue-implant interface at 6 weeks after subcutaneous implantation of 30-mm disks of each surface texture into Sprague-Dawley rats. The scale bars at the bottom of the histology figures represent 500 µm and 100 µm, respectively.

required for tissue-implant separation generally increased with increasing complexity of surface texture. The peak force was approximately 0.3 N for Allergan Smooth and Motiva VelvetSurface, 0.5–0.6 N for Allergan Microcell and Mentor Siltex, and 0.9–1.9 N for Sientra True and Allergan Biocell. The peak force for surfaces with the greatest area was variable (0.5 N for Polytech POLYtxt, 1.7 N for Nagor Nagotex, and 4.6 N for Polytech Microthane). The adherence force required for separation was significantly greater for the Polytech Microthane than for the other textures ($P < 0.05$). The adherence force for the Allergan Biocell and Nagor Nagotex textures differed significantly (all $P < 0.05$) from the textures with lower surface area (Allergan Smooth, Motiva VelvetSurface, Allergan Microcell, and Mentor Siltex), with Biocell also

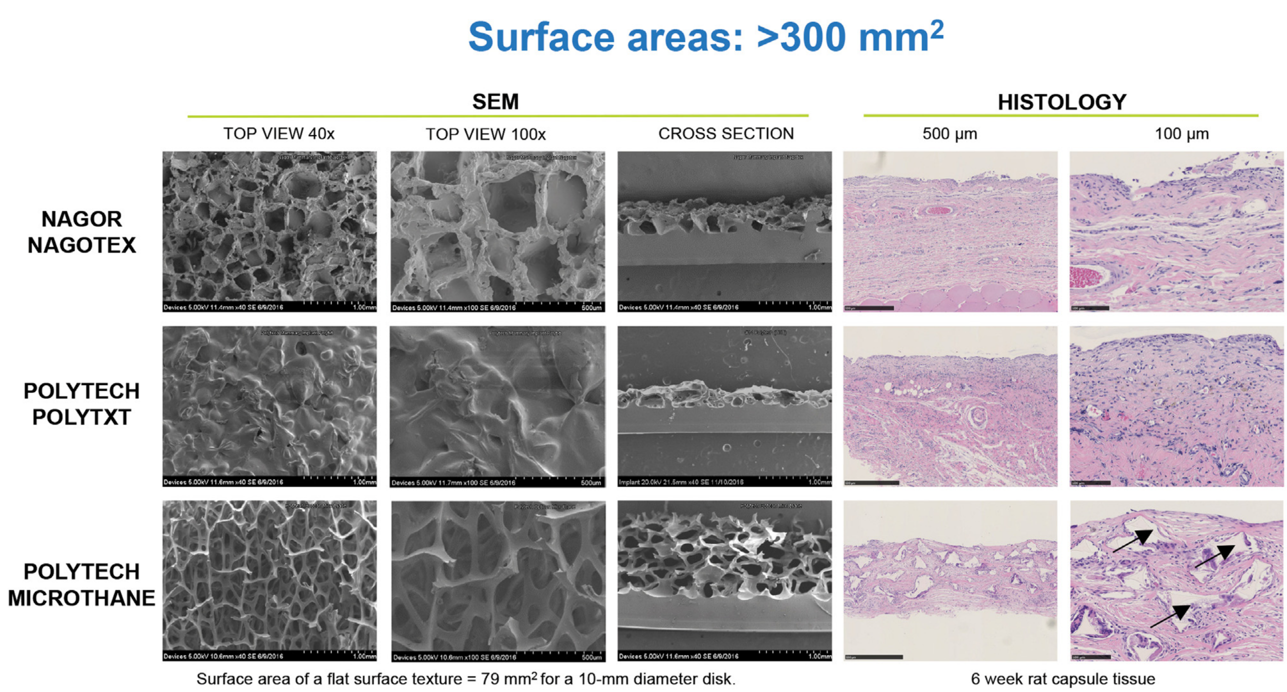

Fig. 5. Left panels show SEM images of the top view (40× and 100×) and cross section of Nagor Nagotex, Polytech POLYtxt, and Polytech Microthane textures. Surface areas were > 300 mm^2. Right panels show representative H&E-stained slides of the capsule at the tissue-implant interface at 6 weeks after subcutaneous implantation of 30-mm disks of each surface texture into Sprague-Dawley rats. The scale bars at the bottom of the histology figures represent 500 µm and 100 µm, respectively. In the H&E stained slides for Polytech Microthane, the clear material identified by the arrows represent texture material.

Table 2
Texture surface area from anterior and posterior of the shell of each breast implant surface texture determined by X-ray computed tomography.

Implant texture	Mean (SD) texture surface area (mm^2) Anterior	Posterior	Mean % greater texture surface area than flat surface[a] Anterior
Allergan Smooth[b]	85 (4)	85 (4)	9
Motiva SilkSurface	85 (1)	85 (2)	8
Motiva VelvetSurface	90 (2)	89 (2)	14
Polytech MESMOsensitive	115 (7)	119 (5)	47
Mentor Siltex	125 (4)	143 (8)	60
Allergan Microcell	145 (4)	132 (12)	85
Allergan Biocell	213 (10)	248 (7)	171
Sientra True	218 (6)	244 (16)	178
Eurosilicone Cristalline	293 (8)	307 (17)	273
Nagor Nagotex	337 (9)	278 (12)	329
Polytech POLYtxt	347 (16)	431 (37)	341
Polytech Microthane	551 (21)	585 (46)	602

SD, standard deviation.
[a] Surface area of a flat surface texture is 79 mm^2 for a 10-mm diameter disk.
[b] The inside of the shell is not flat and contributes to the overall surface area.

significantly different compared with Mentor Siltex ($P < 0.05$).

4. Discussion

Our study is unique in that it connects the physical properties of an implant to in vivo physical performance and tissue morphology. The histological observations help to provide the biological context for the quantitative measurements and the foundation for a better understanding of the role of implant surface texture features in the clinical setting. Other studies have included imaging analyses and in vitro assessment of fibroblast, macrophage, or bacterial adhesion to the shell surface, but have not related these factors to in vivo data (Barr et al., 2009, 2017; Jones et al., 2018; Valencia-Lazcano et al., 2013). Characterizing the physical properties of implant surfaces is key to understanding how a surface texture may impact tissue response to a breast implant. The topography and surface area of 12 implant surface textures from seven different manufacturers were characterized using SEM and X-ray CT imaging. The differences in surface texture may reflect differences in the manufacturing process for each implant (Chao et al., 2016). For example, the Allergan Microcell, Allergan Biocell, Nagor Nagotex, and Eurosilicone Cristalline textures are made by exposing the silicone shell to salt before curing. Although they have similar open pore-like structures, they differ in surface roughness and pore depth, because the salt is removed in a different manner during the manufacturing of each texture. In comparison, the Mentor Siltex surface texture is created using a pressure stamping technique (Chao et al., 2016). The Polytech Microthane texture is made of polyurethane and is manufactured using a different process compared with all other implants in this study. As a result, its appearance is dissimilar to the other textures, with a thin interconnected skeletal framework that creates a much deeper texture. It is important to recognize that all of the surface textures are very different from one another, and the use of texture surface area is just one way to compare them. Other evaluations of the implant surface, such as roughness, are still to be made and will allow for more comprehensive comparisons. This is especially true for smoother-textured surfaces where subtle differences in the evenness of the surface texture may not be fully discernible by the X-ray CT due to the resolution setting of the machine (15 µm) (ASTM International, 2011). This study did not examine the potential role of the differences in chemical composition of the implant surfaces and thus no conclusions can be drawn regarding impact of these differences on the results.

SEM imaging shows that, while the surface characteristics of the textures varied (i.e., pore size, pore number), the depth and complexity of textures allow for groupings based on similarities in texture appearance and depth. The groupings also reflect ranges of the surface texture area as determined by X-ray CT. Consequently, we propose four classifications of textures (smooth/nanotexture, microtexture, macrotexture, and macro-plus texture) based on similarities in visual observations and surface area measurements, with the surface area and degree of texturing and depth increasing with each classification (Fig. 7). The smooth/nanotexture grouping reflects the similarity of the texture depth among members of this classification, although surface roughness may be somewhat greater for a nanotexture compared with a smooth surface texture. This grouping includes devices with a texture surface area of 80–100 mm^2 and consists of Allergan Smooth, Motiva SilkSurface, and Motiva VelvetSurface; microtexture includes devices with a texture surface area of 100–200 mm^2 and consists of Polytech MESMOsensitive, Mentor Siltex, and Allergan Microcell; macrotexture includes devices with a texture surface area of 200–300 mm^2 and consists of Allergan Biocell, Sientra True, and Eurosilicone Cristalline; and macrotexture-plus includes devices with a texture surface area more than 300 mm^2 and consists of Nagor Nagotex, Polytech POLYtxt and Polytech Microthane.

Using SEM and laser confocal imaging, Barr and colleagues classified 13 commercially available textures based on surface roughness into

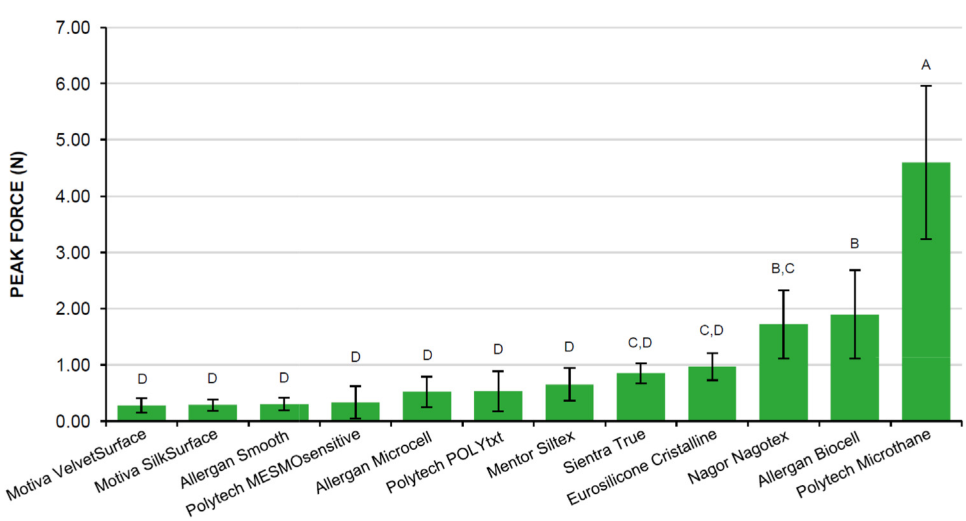

Fig. 6. Mean ± SD adherence force required to separate the tissue capsule from the implant surface assessed 6 weeks after implantation of the different surface textures in Sprague-Dawley rats. N = 8 for each texture. Means that do not share a letter are significantly different ($P \le 0.05$).

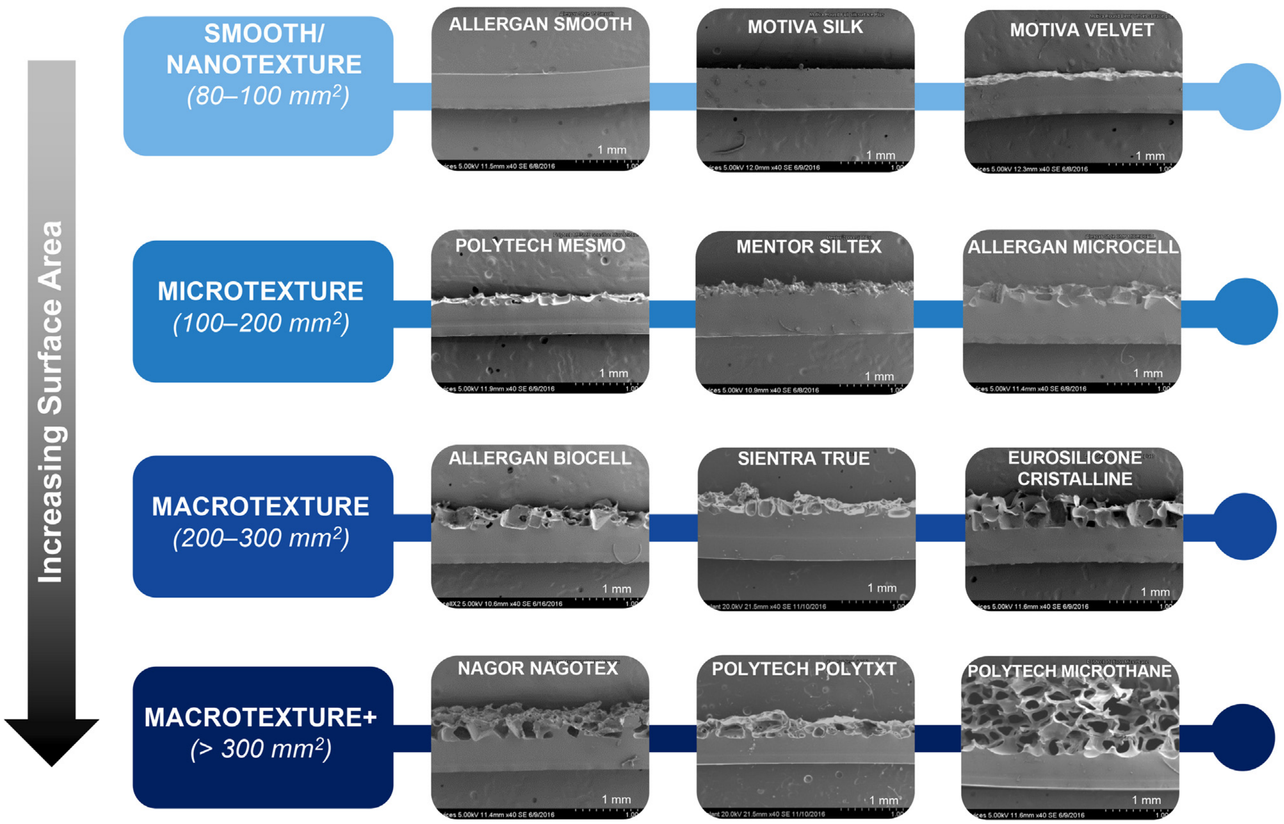

Fig. 7. Classification of implant textures based on texture surface area. SEM images of the cross section of each implant texture are organized into categories according to the magnitude of the texture surface area measured from the anterior of the shell by X-ray computed tomography.

four main groupings, which they termed nano, meso, micro, and macro textures (Barr et al., 2017). The presence of an overhang associated with pores was used to subclassify the microtexture and macrotexture classifications. The classification system described herein does not correspond directly with that reported by Barr et al., likely reflecting differences in implant surfaces examined, methodology, and parameters used to characterize surface texture. Information obtained on topographical evaluation of textured breast implants depends on the methodology used, with a recent study suggesting that white light interferometry may serve as an alternative to laser confocal imaging (Garabedian et al., 2017). Nonetheless, the classifications proposed in the current study and in Barr et al. provide a conceptual framework around the variety of available implants to assist with communication between surgeons and researchers, and to potentially assist surgeons in choosing the right implant to meet patient needs.

In addition to helping classify the implant surface textures, the surface area results of the current study also address questions regarding the variability of the texture across a single implant. Within a single implant, low variability in texture surface area was seen among the multiple samples taken from the anterior of the shell, and separately, among the multiple samples taken from the posterior of the shell. Statistically significant differences in texture surface area between the anterior and posterior of the shell were seen for four of the implants (Mentor Siltex, Allergan Biocell, Nagor Nagotex, and Polytech POLYtxt) with the greatest difference observed with the Polytech POLYtxt implant shells. These differences may not be clinically relevant in that the tissue adherence data show that large disparities in texture surface area between implants do not always result in a statistical difference in tissue adherence (e.g., tissue adherence for the more complex Sientra TRUE texture is not significantly greater than the tissue adherence for the less complex Mentor Siltex texture). The variability in implant textures between the anterior and posterior of the shell is most likely due to the processes used to manufacture the different implant textures. Even though there were differences in texture surface area between the anterior and posterior, the classification of each surface texture remained the same, except for the Nagor Nagotex and Eurosilicone Cristalline. Nagor Nagotex was classified as macrotexture-plus based on the anterior measurement, but would have been classified as macrotexture based on the posterior measurement. The opposite was seen for Eurosilicone Cristalline.

The histology results of this study provide visualization of the tissue integration and show that textures within a given surface area classification had similar capsule morphology, supporting the proposed groupings. The fibrous capsule reflected the surface texture, with an organized fiber structure parallel to the surface of the smooth/nanotexture implants and a disrupted, more disorganized structure found with the macrotexture and macrotexture-plus implants. Specifically, tissue ingrowth increased with increasing complexity of surface texture from smooth/nanotexture to macrotexture-plus. In those implants tested, the peak force required for tissue-implant separation generally increased with surface-texture classification from smooth/nanotexture to microtexture to macrotexture. Two of three surface textures in the macrotexture-plus classification also required high peak force to separate the implant from the tissue. However, the Polytech POLYtxt was an outlier, in that it was classified as macrotexture-plus on the basis of surface area but exhibited tissue adherence similar to that for members of the microtexture classification. On SEM, a cross section of the surface texture of POLYtxt showed large, almost fully enclosed pores in the texture whereas a view of the top surface showed an undulating surface with little to no depth (which was similar to that of a smooth/nanotexture surface). Although the enclosed pores contributed to measurement of the overall surface area of the texture, the lack of depth and openness on the texture surface likely accounted for the minimal tissue adherence.

Previous studies have shown that the tissue capsule forming around an implant mirrors the surface texture pores with which it comes into contact (Nicholson et al., 2007). The macrotexture and macrotexture-plus surfaces have the deepest pores and largest pores based on visual observation, and consequently allow more tissue integration (with the exception of POLYtxt), as reflected by the larger tissue projection along the capsule-implant interface and the greater force required to separate the tissue from the shell material. Smooth/nanotexture implants have a smooth and irregular microstructure with no pores, which limits the number of sites for tissue ingrowth and consequently reduces the opportunity for tissue adherence to the implant. These observations lend substantiation to pore characteristics being the feature of implant surface texture that most impacts tissue adherence. This hypothesis is supported by the comparison of the pores found in the Allergan Microcell and Allergan Biocell textures using quantitative assessments (details provided in Supplementary material). The manufacturing process used for the Biocell texture is designed to create deeper pores than found in the Microcell texture, but the overhang on the surface of Biocell creates a lip over the pore. As a result, surface openness is reduced which allows the tissue to anchor itself into the deeper pores (Barr et al., 2017), resulting in greater tissue adherence with the Biocell texture than the Microcell texture. The greatest tissue adherence was demonstrated by Polytech Microthane, a polyurethane-coated implant, which also exhibited a unique capsule morphology that differed from the other implants in the macrotexture-plus classification. Although the chemical composition of this implant may contribute to these observations, further research would be required to distinguish the relative contributions of surface texture topography and chemical composition. While strong tissue adherence and a unique pattern of tissue integration could be clinically desirable, the polyurethane coating on currently available implants has been shown to degrade over time (Castel et al., 2015). The development of an implant with a similar open pore structure that retains its structural integrity and provides the desired biological and clinical performance could be a focus for future implant design. A new subcategory of implants defined by their unique pore structure might result from the availability of such an implant.

5. Conclusions

The data from this study show that variations in implant surface texture directly affected capsule structure and morphology, and in turn, influenced capsule adherence to the implant. Increasing complexity of the surface texture can markedly alter the pathophysiology of the foreign body response, leading to more tissue ingrowth, which disrupts capsule fiber organization and increases tissue adherence. Surface area is, therefore, an important factor contributing to tissue ingrowth and adherence. These findings provide a better understanding of the landscape with respect to the surface texture properties of breast implants, thus enabling the classification of the implants evaluated in this study into groups based on their surface characteristics.

Acknowledgments

Writing and editorial assistance was provided to the authors by Peloton Advantage, Parsippany, NJ, and was funded by Allergan plc, Dublin, Ireland. Neither honoraria nor other form of payments were made for authorship.

Role of funding source

This study was sponsored by Allergan plc, Dublin, Ireland. Michael Atlan, Gina Nuti, Hongpeng Wang, Sherri Decker, and TracyAnn Perry participated in the development of the study design; in the collection, analysis and interpretation of data; in the writing of the report; and in the decision to submit the article for publication.

Author disclosures

Michael Atlan is a consultant for workshops and has developed educational presentations for Allergan.

Gina Nuti is an employee of Allergan plc.

Hongpeng Wang is an employee of Allergan plc.

Sherri Decker is an employee of Allergan plc.

TracyAnn Perry was an employee of Allergan at the time of study conduct and manuscript preparation.

Appendix A. Supporting information

Supplementary data associated with this article can be found in the online version at doi:10.1016/j.jmbbm.2018.08.035.

References

ASTM International, 2011. Standard Guide for Computed tomography (CT) Imaging Designation: E1441–11. ASTM International, West Conshohocken, PA.

Atlan, M., Bigerelle, M., Larreta-Garde, V., Hindie, M., Hedén, P., 2016. Characterization of breast implant surfaces, shapes, and biomechanics: a comparison of high cohesive anatomically shaped textured silicone, breast implants from three different manufacturers. Aesthet. Plast. Surg. 40, 89–97.

Barnsley, G.P., Sigurdson, L.J., Barnsley, S.E., 2006. Textured surface breast implants in the prevention of capsular contracture among breast augmentation patients: a meta-analysis of randomized controlled trials. Plast. Reconstr. Surg. 117, 2182–2190.

Barr, S., Hill, E., Bayat, A., 2009. Current implant surface technology: an examination of their nanostructure and their influence on fibroblast alignment and biocompatibility. Eplasty 9, e22.

Barr, S., Hill, E.W., Bayat, A., 2017. Functional biocompatibility testing of silicone breast implants and a novel classification system based on surface roughness. J. Mech. Behav. Biomed. Mater. 75, 75–81.

Brohim, R.M., Foresman, P.A., Hildebrandt, P.K., Rodeheaver, G.T., 1992. Early tissue reaction to textured breast implant surfaces. Ann. Plast. Surg. 28, 354–362.

Bui, J.M., Perry, T., Ren, C.D., Nofrey, B., Teitelbaum, S., Van Epps, D.E., 2015. Histological characterization of human breast implant capsules. Aesthet. Plast. Surg. 39, 306–315.

Castel, N., Soon-Sutton, T., Deptula, P., Flaherty, A., Parsa, F.D., 2015. Polyurethane-coated breast implants revisited: a 30-year follow-up. Arch. Plast. Surg. 42, 186–193.

Chao, A.H., Garza 3rd, R., Povoski, S.P., 2016. A review of the use of silicone implants in breast surgery. Expert Rev. Med. Devices 13, 143–156.

Clugston, P.A., Perry, L.C., Hammond, D.C., Maxwell, G.P., 1994. A rat model for capsular contracture: the effects of surface texturing. Ann. Plast. Surg. 33, 595–599.

Danino, A., Rocher, F., Blanchet-Bardon, C., Revol, M., Servant, J.M., 2001. A scanning electron microscopy study of the surface of porous-textured breast implants and their capsules. Description of the "velcro" effect of porous-textured breast prostheses. Ann. Chir. Plast. Esthet. 46, 23–30.

Danino, M.A., Efanov, J.I., Dimitropoulos, G., Moreau, M., Maalouf, C., Nelea, M., Izadpanah, A., Giot, J.P., 2018. Capsular biofilm formation at the interface of textured expanders and human acellular dermal matrix: a comparative scanning electron microscopy study. Plast. Reconstr. Surg. 141, 919–928.

del Rosario, A.D., Bui, H.X., Petrocine, S., Sheehan, C., Pastore, J., Singh, J., Ross, J.S., 1995. True synovial metaplasia of breast implant capsules: a light and electron microscopic study. Ultrastruct. Pathol. 19, 83–93.

Derby, B.M., Codner, M.A., 2015. Textured silicone breast implant use in primary augmentation: core data update and review. Plast. Reconstr. Surg. 135, 113–124.

Efanov, J.I., Giot, J.P., Fernandez, J., Danino, M.A., 2017. Breast-implant texturing associated with delamination of capsular layers: a histological analysis of the double capsule phenomenon. Ann. Chir. Plast. Esthet. 62, 196–201.

Garabedian, C., Delille, R., Deltombe, R., Anselme, K., Atlan, M., Bigerelle, M., 2017. A multi-topographical-instrument analysis: the breast implant texture measurement. Surf. Topogr. 5, 025004.

Hakelius, L., Ohlsen, L., 1992. A clinical comparison of the tendency to capsular contracture between smooth and textured gel-filled silicone mammary implants. Plast. Reconstr. Surg. 90, 247–254.

Hakelius, L., Ohlsen, L., 1997. Tendency to capsular contracture around smooth and textured gel-filled silicone mammary implants: a five-year follow-up. Plast. Reconstr. Surg. 100, 1566–1569.

Harvey, A.G., Hill, E.W., Bayat, A., 2013. Designing implant surface topography for improved biocompatibility. Expert Rev. Med. Devices 10, 257–267.

Headon, H., Kasem, A., Mokbel, K., 2015. Capsular contracture after breast augmentation: an update for clinical practice. Arch. Plast. Surg. 42, 532–543.

Jones, P., Mempin, M., Hu, H., Chowdhury, D., Foley, M., Cooter, R., Adams Jr, W.P., Vickery, K., Deva, A.K., 2018. The functional influence of breast implant outer shell morphology on bacterial attachment and growth. Plast. Reconstr. Surg (In Press).

Kappel, R.M., Klunder, A.J.H., Pruijn, G.J.M., 2014. Silicon chemistry and silicone breast implants. Eur. J. Plast. Surg. 37, 123–128.

Landis, E.N., Keane, D.T., 2010. X-ray microtomography. Mater. Charact. 61, 1305–1316.

Maxwell, G.P., Gabriel, A., 2017. Breast implant design. Gland Surg. 6, 148–153.

Maxwell, G.P., Scheflan, M., Spear, S., Nava, M.B., Hedén, P., 2014. Benefits and

limitations of macrotextured breast implants and consensus recommendations for optimizing their effectiveness. Aesthet. Surg. J. 34, 876–881.
Minami, E., Koh, I.H., Ferreira, J.C., Waitzberg, A.F., Chifferi, V., Rosewick, T.F., Pereira, M.D., Saldiva, P.H., de Figueiredo, L.F., 2006. The composition and behavior of capsules around smooth and textured breast implants in pigs. Plast. Reconstr. Surg. 118, 874–884.
Nicholson, K., Abramova, L., Chren, M.M., Yeung, J., Chon, S.Y., Chen, S.C., 2007. A pilot quality-of-life instrument for acne rosacea. J. Am. Acad. Dermatol. 57, 213–221.
Sheikh, Z., Brooks, P.J., Barzilay, O., Fine, N., Glogauer, M., 2015. Macrophages, foreign body giant cells and their response to implantable biomaterials. Materials 8, 5671–5701.
Valencia-Lazcano, A.A., Alonso-Rasgado, T., Bayat, A., 2013. Characterisation of breast implant surfaces and correlation with fibroblast adhesion. J. Mech. Behav. Biomed. Mater. 21, 133–148.
Yeoh, G., Russell, P., Jenkins, E., 1996. Spectrum of histological changes reactive to prosthetic breast implants: a clinicopathological study of 84 patients. Pathology 28, 232–235.